Sensors and Electronic Instrumentation Advances

Proceedings

of the 7th International Conference on Sensors and Electronic Instrumentation Advances (SEIA' 2021)

Edited by Sergey Y. Yurish

MALLORCA
SEIA'21

Sensors and Electronic Instrumentation Advances:

Proceedings of the 7th International Conference on Sensors and Electronic Instrumentation Advances

22-24 September 2021
Palma de Mallorca, Mallorca (Balearic Islands), Spain

Edited by Sergey Y. Yurish

IFSA Publishing

Contents

(018)

Fiber-optic Mach-Zehnder Interferometer for Refractive Index Measurement Based on MEMS Optofluidic Platform

Z. Djinović [1], A. Kocsis [1] and M. Tomić [2]
[1] ACMIT Gmbh, 2 Viktor Kaplan str., 2700 Wiener Neustadt, Austria
[2] Institute of Technical Sciences of SASA, 35 Knez Mihailova, 11000 Belgrade, Serbia
Tel.: + 436644669297
E-mail: zoran.djinovic@acmit.at

Summary: We present a fiber-optic sensing configuration based on Mach-Zehnder interferometer (MZI) embedded into the MEMS optofluidic platform for measurement of index of refraction of liquids in dynamic regime. The sensing principle is based on the low-coherence interferometry, characterized by generation of Gaussian shape interferograms, which maximum position depends on the optical path difference (OPD) between the sensing and reference arm of the MZI. When liquid flows through the central microchannel of the optofluidic platform it crosses the light beam between the two optical fibers in the sensing arm causing the OPD change. An algorithm has been applied for calculation of index of refraction of liquids out of the raw interference signals. We obtained very good agreement between the experimental results and literature data of index of refraction of subjected fluids. The accuracy of index of refraction measurement is about 1 % that is predominantly determined by accuracy of reading the position of mechanical scanner.

Keywords: Fiber-optic sensors, Index of refraction, Interferometry, Optofluidic, MEMS.

1. Introduction

Index of refraction is a frequently used physical parameter for material characterization in various scientific and industrial fields including life science, biomedicine, analytical chemistry and bio-chemistry, material science, etc. [1, 2]. Fiber-optic sensors for refractive index measurement have attracted attention of many research groups dealing with label-free biological and biochemical sensing since they provide high sensitivity, fast response, extremely small volume of test sample, remote sensing, immunity against electromagnetic radiation, etc. [3]. Among them fiber-optic interferometric sensors are the most sensitive and allow different designs [4, 5]. They are very convenient to combine with some other technologies such as micro-electro-mechanical-systems (MEMS) for making high throughput analytical devices such as Lab-on-a-Chips and micro total analyser system (m-TAS) [6]. These systems allow a number of advantages such as direct contactless detection, miniaturization and multiplexing.

In this paper, we present a sensing configuration for in-line measurement of index of refraction of liquid samples based on low-coherence Mach-Zehnder interferometer (MZI), embedded into the MEMS optofluidic platform. The MZI is built up of two 1×2 single-mode fiber-optic couplers. The optofluidic platform is composed of glass and silicon wafers, which are anodically bonded. The structure contains a central microchannels, which enable the flow of a liquid sample through the platform. In the down side of the platform there are V-grooves which holds the sensing optical fibers. The reference fiber is mechanically moved along its groove, changing the optical path difference of MZI. We applied the centroid algorithm for finding out the center of the coherence zone in the low coherence interferogram. We measured index of refraction of five liquids and got a very good agreement between the experimental results and literature data.

2. Principle of Operation

Fig. 1 presents a sensing configuration based on single-mode @1310 nm "all-in-fiber" low-coherence Mach-Zehnder interferometer (MZI) integrated in an MEMS optofluidic platform.

This is a two beams interferometer, containing two beam splitters, with two completely separated paths. Intensity of light at the interferometer output is described by classical interferometric relation [7]:

$$I_D = I_1 + I_2 + 2\sqrt{I_1}\sqrt{I_2}\,|\gamma_{11}(\Delta L_{12})|\cos\left[\frac{2\pi}{\lambda}\Delta L_{12}\right], \quad (1)$$

where I_1 and I_2 are irradiances of light beams in the two interferometric arms; $\Delta L_{12} = L_1 - L_2$ is the optical paths difference (OPD) of the two light beams; $\gamma_{11}(\Delta L_{12})$ is light source degree of coherence. Optical paths L_1 and L_2 are obtained by integration along two separated paths, from the first fiber optical coupler, throughout two fibers, till the second, combining optical coupler.

The principle of operation of MZI in a low coherence sensing application is as following. The lengths of two arms are made to be approximately equal, within several hundreds of micrometers. One of the interferometer arms, named the sensing arm, is exposed to the influence of a measurand. This measurand (and preferably only this one) changes, in

some way, the optical path inside this arm (e.g. by changing the index of refraction or physical length of the fiber). In the other interferometer arm, called the reference arm, the optical path has been changed in a controllable way. The simplest technique to do that is mechanical scanning of the air gap between the two fiber ends.

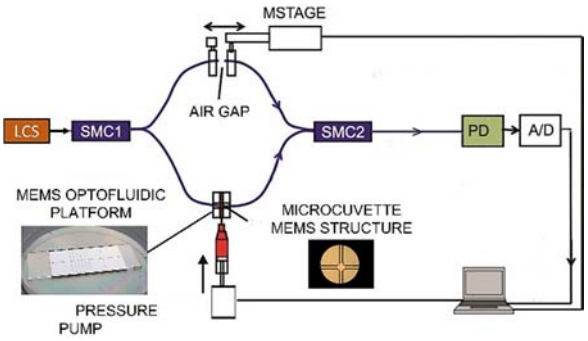

Fig. 1. Schematic presentation of fiber-optic Mach-Zehnder interferometer sensing configuration and MEMS platform. LSC – low coherence source, SMC1,2 – single mode fiber optic coupler, PD – photodetector, A/D – acquisition card, MSTAGE – motorized stage.

Superluminescent diode is a light source frequently used in a low coherence interferometric configuration due to relatively large spectral width and consequently relatively low coherence length. When such a source is employed, the interferometric term in Eq. (1) (containing the degree of coherence $\gamma_{11}(\Delta L_{12})$) decreases rapidly with ΔL_{12} augmentation. The maximum of interferometric term is reached when $\gamma_{11}(\Delta L_{12})$ equals one, i.e. when the interferometer OPD equals zero. Scanning the air gap in the reference arm, this position - L_{SC1}, where the interferometer OPD equals zero, can be found as a maximum of interferometric term. If the air gap width is L_{AIRGAP}, and the difference in fiber arm length ΔL_{FIB}, the OPD equals zero in position:

$$L_{SC1} = L_{AIRGAP} + \Delta L_{FIB} \tag{2}$$

If the air gap in the sensing arm is now filed with an examined liquid, the position of zero OPD moves in L_{SC2} position given by:

$$L_{SC2} = n_{LIQUID} \cdot L_{AIRGAP} + \Delta L_{FIB}, \tag{3}$$

where n_{LIQUID} is the refractive index of liquid, at the wavelength of light source.

Combining Eq. (2) and Eq. (3), the refractive index can be calculated from these two measured positions of zero OPD, L_{SC1} and L_{SC2}:

$$n_{LIQUID} = \frac{1}{L_{AIRGAP}}(L_{SC2} - L_{SC1}) + 1 \tag{4}$$

The precision and accuracy of the index measurement are determined by the precision and accuracy of measurement of the zero OPD, L_{SC1} and L_{SC2} (we assume that the width of the air channel, made by MEMS technique, is fixed and very accurate measured). The measurement of the zero OPD is a challenging task, which include another several assumptions and procedures. The first assumption is that we knows exactly the central wavelength of the low coherence source (LCS). The second is that we can scan the OPD by moving the reference fiber with a constant, accurately measured speed. An alternative to this assumption is having a method to accurately measure the position of the fiber during the scanning. This can be achieved by an independent (opto-) mechanical encoder, or by using an additional high coherence laser beam in the same time and with the same path as the LCS. Procedures for determining the zero OPD are numerous, from the simple identification of the maximal interferogram value, the envelope fitting [8], the centroid algorithm [9], to the most complex application of the FFT [10-12] and wavelet transformations [13]. In this work we used the centroid algorithm, where the position L_{SC} of the fringe pattern was calculated using the following equation [14]:

$$L_{SC} = \frac{\sum_{|I(L_p)|\geq 0.3 I_{max}} L_p \cdot |I(L_p|}{\sum_{|I(L_p)|\geq 0.3 I_{max}} |I(L_p)|}, \tag{5}$$

where L_p is the point position of the fringe pattern, $I(L_p)$ is the intensity value of the point and I_{max} is the maximal value of the fringe points.

3. Design of the Optofluidic Platform

Fig. 2a presents the final design of the optofluidic platform that is used for the fluid flow simulation. The platform consists of one central microchannel for the testing fluid and five orthogonal channels. The first one at the right side of the platform serves for the reagent transportation, while the rest four are aimed for integration of different fiber-optic sensors. In this investigation we used just one orthogonal channel equipped with sensing fibers of a MZI.

The platform consists of a silicon chip with overall dimensions of 50×25×0.42 mm, anodically bonded to a pyrex glass with overall dimensions of 75×25×1.12 mm. The dimensions of the glass plate correspond to the standard microscopic glass plate and will be suitable for the inspection purposes. The width of the channels for both fluid flow and fiber insertion is 245 μm, measured at the channel top. The channels are V-shaped, determined by the (111) crystallographic planes. The cross section of the channels for both fluid flow and fiber insertion is given in Fig. 2b and Fig. 2c shows the channel's crossovers.

We performed 3D simulation of the fluid flow through the whole structure to determine what relative pressures are needed at the inlet of the structure in order to attain a certain fluid velocity in the central microchannel. We assumed that the flow through the

system is laminar. The inlet flow is fully developed laminar flow, described by the corresponding inlet boundary condition. The boundary conditions at the inlet and outlet set a constant relative pressure. All other boundaries are solid walls described by a non-slip boundary condition. The fluid used in simulation was pure water with density $\rho = 1000$ kg/m^3 and viscosity $\mu = 0.001$ Pa·s. The simulation is done for four different values of the relative pressure at the inlet [0.001, 0.005, 0.01, 0.05] bar.

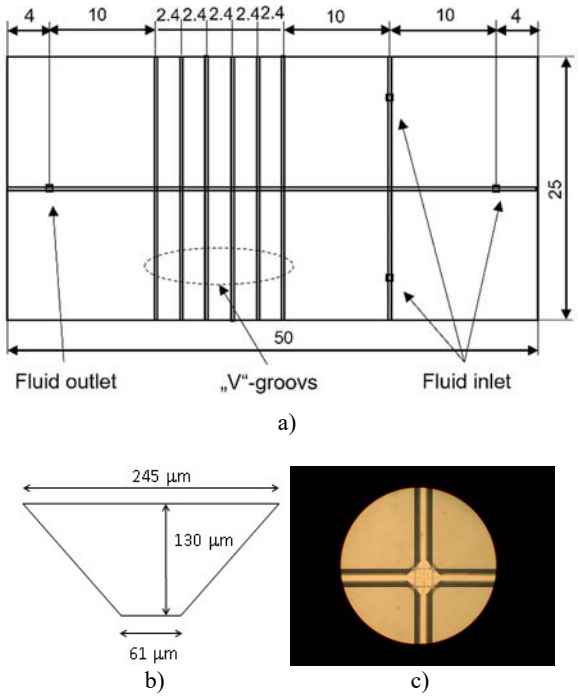

Fig. 2. a) Overall view and dimensions (in mm) of the MEMS structure; b) The cross-section of the micro channels for both fluid flow and fiber insertion; c) The cross-over of the microchannels.

The Laminar Flow user interface is primarily applied to flows of low to intermediate Reynolds numbers ($R < 2000$). In our structure, for pure water as the fluid, the calculated Reynolds number is less than 1 and the laminar flow condition is fulfilled. Fig. 3 gives the 3D distribution of velocity in the structure for an applied pressure at the inlet of 0.01 bar. As expected, the velocity dependence is parabolic, equal to zero at the structure walls, and its maximum value is reached in the microchannel, which is the narrowest part of the structure.

Fig. 4 shows the dependence of the fluid velocity magnitude in a point in the middle of the microchannel for different values of the relative pressure at the inlet. As seen, the velocity is the largest in the microchannel which is the narrowest part of the structure, and this velocity rises linearly with pressure applied at the inlet (pressure at the outlet = 0 bar).

Numerical simulation allows us to roughly estimate the value of pressure to be applied at the inlet of the microchannel to achieve laminar flow and required speed in the channel. We are also able to follow the change in velocity in the microchannel in places where the channel is extended (channels crossover).

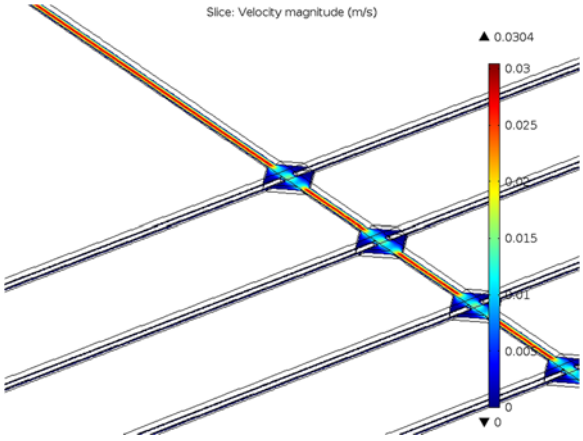

Fig. 3. 3D distribution of velocity in the part of the structure given in Fig. 1 for an applied pressure at the inlet of 0.01 bar.

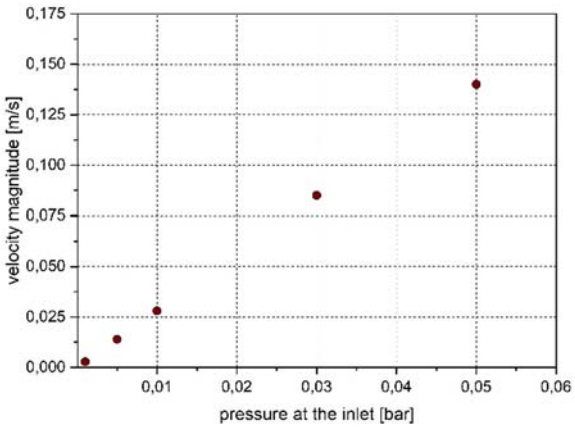

Fig. 4. Dependence of velocity intensity in a point in the middle of the channel on the pressure applied at the inlet.

3. Experiment

Fig. 5 shows an overall view of experimental setup composed in accordance with sensing configuration depicted in Fig. 1. The optofluidic platform, presented in the inset of Fig. 2., is made by anodic bonding of silicone upper plate to the glass bottom plate. Central microfluidic channel and five ”V” groove lateral channels 125 µm in width are made by chemical etching of Si. The platform is set to be just under the optical microscope equipped with video camera and acquisition unit for capturing the streaming fluid through the central microchannel. Before characterization, the Mach-Zehnder interferometer was set to be in equilibrium, i.e. the optical path difference in sensing and reference arm was set to zero (OPD = 0). Usually, it was done by mechanical scanning (Z600 Series Motorized Actuator, ThorLabs, Newton, NJ, USA) and SmartMove Motor Controller Software C-843 Motor (Physik Instrumente (PI),

Karlsruhe, Germany) one of the fibers in the reference arm and by simultaneous acquisition of the InGaAs photodiode (Roithner Lasertechnik, Vienna, Austria) signal (see Fig. 1). The subjected fluids have been supplied into the microchannel of the optofluidic platform by air driven pump (Flow EZ 7000 mbar, Fluigentat, France) at 2 bar.

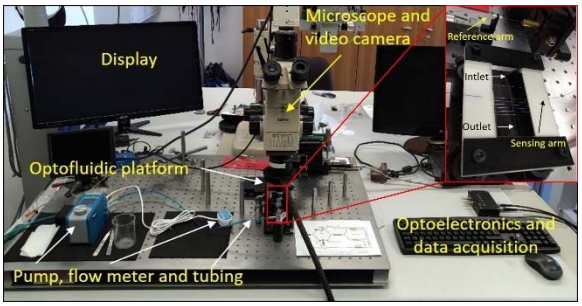

Fig. 5. Experimental setup with optofluidic MEMS platform. Inset: close look of the platform.

3. Results and Discussions

Fig. 6 presents two Gaussian shape low-coherence interferograms (LCI) acquired by measuring of index of refraction of isopropanol. The first LCI relates to air (L_{SC1}) and second one (L_{SC2}) to isopropyl alcohol which is introduced into the microcavity of the optofluidic platform. In the same way the LCIs of distilled water, ethanol, methanol and 0.9 % NaCl solutions were obtained. Index of refraction of subjected liquids was calculated out of measured OPDs (L_{SC2} and L_{SC1}) and the width of the channel (L_{AIRGAP}), using Eq. (4).

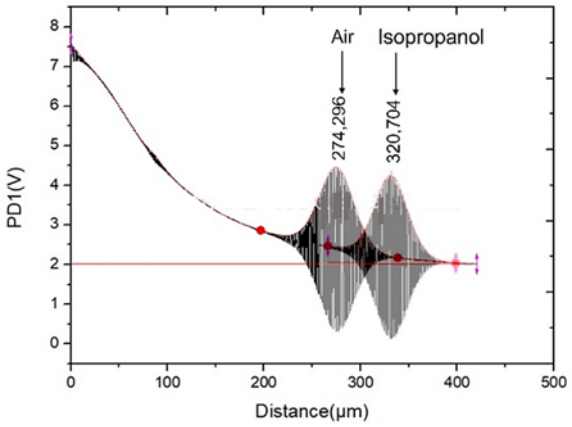

Fig. 6. Low-coherence interferograms of acquired by scanning of microcavity of optofluidic platform filled with air (1st LCI) and with isopropyl alcohol (2nd LCI).

The OPD was calculated as the product of the scanning speed and the time from the begging of the scanning to the moment when the center of coherence zone occurs. The onset of the scanning was accurately and very repeatable detected as the moment when the first interferometric fringe starts to rise up, indicating in that way the detachment of the fiber's tips. This small zone of the interferometric fringes can be noticed in Fig. 6, in the very beginning of the photodetector signal.

We applied the centroid algorithm in several steps. The first one was the band-pass filtration, when the quasi DC component and the high-frequency noise were removed. In the second step, the local maxima of interferometric friges were detected. The example of the interferogram at the end of the second phase is presented in Fig. 7.

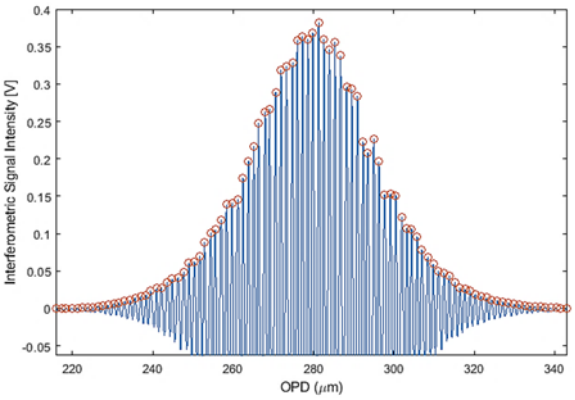

Fig. 7. Low-coherence interferogram after band-pass filtration. The local maxima are detected and marked by (o).

The position of the center of the coherence zone for the air gap L_{SC1} was declared as the zero position where the refractive index equals to 1. Thus, the accuracy of the measurement of L_{SC1} (mean value) is 100 % by definition. Results of measurement of index of refraction of the aforementioned fluids are depicted in Fig. 8, along with the literature data from [15].

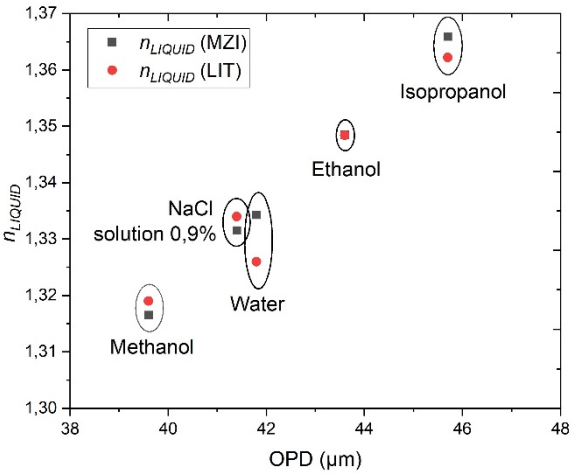

Fig. 8. Index of refraction of subjected fluids obtained by MZI interferometer (■) and literature data (LIT) (●).

A very good agreement between our experimental results (MZI) and literature data (LIT) was obtained. In the fluid refractive index measurements we obtained the mean absolute error of 0.0034, with standard deviation of 0.0037. The relative measurement uncertainty calculated in respect to the value of 0.35, which was taken as the mean effectively measured

index value (1.35-1), was about 1 % (0.0034/0.35). One exception was the measurement of the distilled water, where we measured its refraction index with the absolute error of 0.0083 (2.5 %).

It is interesting to note that the standard deviations in 16 measurements performed with the air filled channel was only 0.0002 – one order of magnitude better than in the measurement with fluids. This result can lead to the conclusion that the precision and accuracy of measurement can be better than those of 1 %, which we found out in this measurement, using the same scanning mechanism and the centroid algorithm.

4. Conclusions

We presented a fiber-optic sensing technique capable to measure index of refraction of liquids in dynamic regime. The technique combines a Mach-Zehnder low-coherence interferometer embedded into the MEMS optofluidic platform. Five liquids were tested with index of refraction in the range of 1.32 to 1.38. A very high agreement between the experimental and literature data was obtained. The precision and accuracy of the index of refraction measurement was about 1 %. The proposed sensor is suitable for label-free sensing in biomedicine due to high precision and accuracy and small sample volume.

Acknowledgements

The authors thank to the NFB und ACMIT Gmbh, Austria, which sponsored this work in the frame of the LSC15-004 project “Immune-regulatory capacity of mesenchymal stem cells (MSCs)”. M.T. thanks to Ministry of Education, Science and Technological Development of Serbia to support him in this investigation, in the frame of the agreement 451-03-68/2020-14/200175 with ITS-SASA.

References

[1]. J. A. Flores-Bravo, M. A. Illarramendi, J. Zubia, J. Villatoro, Optical fiber interferometer for temperature-independent refractive index measuring over a broad range, *Optics and Laser Technology*, Vol. 139, 2021, 106977.

[2]. S. Samanta, S. Kalathimekkad, S. K. Selvaraja, Fluid sensing strategies adopted in photonic devices: A review, *Optics and Laser Technology*, Vol. 139, 2021, 106975.

[3]. J. T. Dong, C. H. Cheng, C. Wu, J. Li, B. O. Guan, Highly sensitive optofluidic refractive index sensor based on a seven-liquid-core Teflon-cladding fiber, *Optics Express*, Vol. 28, Issue 18, 2020, pp. 26218-26227.

[4]. J. Jiang, Y. Zhao, Y. Yang, Y. Wang, X. He, W. Yang, L. Li, All-fiber Fabry-Perot interferometer for liquid refractive index measurement, *Journal of Russian Laser Research*, Vol. 40, Issue 4, 2019, pp. 370-374.

[5]. H. Yu, L. Xiong, Z. Chen, Q. Li, X. Yi, Y. Ding, F. Wang, H. Lv, Y. Ding, Ultracompact and high sensitive refractive index sensor based on Mach-Zehnder interferometer, *Optics and Lasers in Engineering*, Vol. 56, 2014, pp. 50-53.

[6]. A. Rostamian, E. Madadi-Kandjani, H. Dalir, V. J. Sorger, R. T. Chen, Towards lab-on-chip ultrasensitive ethanol detection using photonic crystal waveguide operating in the mid-infrared, *Nanophotonics*, Vol. 10, Issue 6, 2021, pp. 1675-1682.

[7]. M. Francon, Optical Interferometry, *Academic Press*, 1966.

[8]. K. Larkin, Efficient nonlinear algorithm for envelope detection in white light interferometry, *J. Opt. Soc. Am.,* Vol. 13, Issue 4, 1996, pp. 832-843.

[9]. C. Ai, E. L. Novak, Centroid Approach for Estimating Modulation Peak in Broad-Bandwidth Interferometry, U. S. Patent 5,633,715, *USA*, 27 May 1997.

[10]. S. Chim, G. Kino, Three-dimensional image realization in interference microscopy, *Appl. Opt.*, Vol. 31, Issue 14, 1992, pp. 2550-2553.

[11]. Q. Vo, F. Fang, X. Zhang, H. Gao, Surface recovery algorithm in white light interferometry based on combined white light phase shifting and fast Fourier transform algorithms, *Appl. Opt.*, Vol. 56, Issue 29, 2017, pp. 8174-8185.

[12]. Z. Yu, A. Wang, Fast White light interferometry demodulation algorithm for low-finesse Fabry-Pérot sensors, *IEEE Photonics Technology Letters*, Vol. 27, Issue 8, 2015, pp. 817-820.

[13]. P. Sandoz, Wavelet transform as a processing tool in white-light interferometry, *Opt. Lett.,* Vol. 22, Issue 14, 1997, pp. 1065-1067.

[14]. C. Wang, X. Zhang, J. Jiang, K. Liu, S. Wang, Y. Li, T. Liu, A demodulation method of spatial domain for low-coherence interferometry with high accuracy and adaptability, *IEEE Photonics Journal*, Vol. 12, Issue 2, 2020, pp. 1-11.

[15]. Refractive Index Database, https://refractiveindex.info/